Materials Today Communications 36 (2023) 106442

Contents lists available at ScienceDirect

Materials Today Communications

journal homepage: www.elsevier.com/locate/mtcomm

Effect of crystallinity and morphology on the mechanical properties of CF/PEKK composites manufactured under compression moulding and automated tape placement

Helena Pérez-Martín [a], Stefan Buchalik-Bopp [b], Barbara E. Guettler [b], Paul Mackenzie [c], Alex Baidak [c], Conchúr M. Ó Brádaigh [a], Dipa Ray [a,*]

[a] School of Engineering, Institute for Materials and Processes, The University of Edinburgh, Edinburgh, United Kingdom
[b] Leibniz-Institut für Verbundwekstoffe GmbH, Kaiserslautern, Germany
[c] Hexcel Composites Ltd., Duxford, Cambridge, United Kingdom

ARTICLE INFO

Keywords:
Polymer-matrix composites (PMCs)
Thermoplastic resin
Mechanical properties
Compression moulding
Automated tape placement
Carbon fibre
PEKK

ABSTRACT

The present work aims to establish to what extent crystallisation morphology and kinetics affect the matrix-dominated properties of CF/PEKK composites, two factors which have been minimally investigated together in existing literature. Different compression-moulding cycles and automated tape placement (ATP) were used as the processing routes. Their effects on void content, crystallinity development, morphology and mechanical performance were investigated. Results showed that ~~all~~ compression-moulded laminates undergoing different isothermal crystallisation conditions achieved similar levels of consolidation and crystallinity, although the spherulitic development varied considerably. The effect of different crystalline structures was not evident on the properties investigated, as all compression-moulded laminates performed similarly. However, ATP laminates displayed a higher void content and low crystallinity, resulting in a lower performance across the investigated mechanical properties. While the modification of some ATP parameters resulted in slight improvements in performance in some testing, the results indicated that a thorough understanding of the correlation between processing conditions and development of crystalline structures in PEKK is needed in order to produce good-quality CF/PEKK parts under very rapid processing conditions and ensure the repeatability of this.

1. Introduction

The use of high-performance thermoplastic matrices in structural composites is of high interest in the aerospace industry. Poly(ether-ketoneketone) (PEKK) in particular is a semicrystalline thermoplastic, attractive due to its excellent mechanical properties, chemical inertness and resistance to high temperatures [1–4]. The range of PEKK grades that can be achieved, allowing manufacturers to choose which grade better suits their application, makes it a versatile and interesting material in industry. Using PEKK, or any other thermoplastic polymer, as a matrix in composites is also advantageous for manufacturers as they have the potential to undergo single-step processing, and have a better starting point to mechanically recycle the components at their end of life.

An example of such a process is automated tape placement (ATP), which is designed for fast production, energy consumption and cost reduction, automation and repeatability of part manufacturing. However, such fast manufacturing techniques (consolidation times of seconds or a fraction of a second [5]) can result in lower quality and performance when compared to slower processing techniques such as compression moulding or autoclaving (consolidation times of 20–60 + minutes [6–8]). The temperature, pressure and environmental control that autoclave manufacturing provides is often considered the golden standard in composite manufacturing. When compared to this, the fast-paced nature of the ATP manufacturing process results in very short exposure times to high temperatures and pressures. This limits the time window for resin flow, adhesion between the laid plies and void reduction, which are factors that play key roles in consolidation quality, part integrity and properties [5,6,9–11].

The use of thermoplastics for in-situ manufacturing comes with several challenges regarding their processing. Thermoplastics possess high viscosities in molten conditions when compared to thermosetting

* Correspondence to: 1.140 Sanderson Building King's Buildings, Edinburgh EH9 3FB, Scotland, UK.
E-mail address: Dipa.Roy@ed.ac.uk (D. Ray).

https://doi.org/10.1016/j.mtcomm.2023.106442
Received 28 April 2023; Received in revised form 6 June 2023; Accepted 13 June 2023
Available online 14 June 2023

resins, hindering fibre impregnation, interply contact and polymer chain reptation. The processing conditions add a further layer of complexity in the case of semicrystalline thermoplastics such as PEKK, as their crystallinity content and morphology are dependent on the thermal history that the part undergoes. This in turn affects the mechanical and chemical performance of the manufactured part, which are critical in high-performance applications such as aerospace [5,12,13].

Consequently, optimising the processing parameters is of paramount importance for thermoplastics, particularly offering temperature and pressure control and exposure times catered to the material being used. It is common to perform some form of secondary processing, involving reheating and reconsolidation of ATP-manufactured thermoplastic composite parts to improve mechanical performance [10,14]. In the case of CF/PEKK, a previous study has shown an improvement in crystallinity and reduction in void content with increasing number of layers as a consequence of repeated heat exposure and slower cooling profiles when further away from the lay-down surface [15]. In order to fully optimise the processing of such materials, however, it is important to establish an understanding of the effect of thermal history on the morphology and properties of the composite matrix.

Differential scanning calorimetry (DSC) studies have shown a dual melting behaviour in both unreinforced and CF-reinforced PEKK after undergoing isothermal crystallisation [1–3,16–20], also observed in the widely-studied poly(etheretherketone) (PEEK) [21–26]. This consists of a lower temperature endotherm (LTE) that varies in temperature and area based on the isothermal hold temperature, and a higher temperature endotherm (HTE) corresponding to conventional melting that takes place at the same temperature (~336 °C) irrespective of thermal history. This suggests there are two different crystal structures present with different thermal stability, one of them being more reliant on the material's thermal history. In literature, these have been assigned to primary and secondary crystallisation, where the primary spherulitic structure forms first, followed by a secondary slower interlamellar crystallisation once the primary structure is established. The latter has slower kinetics and its thermal stability is dependent on the processing conditions, hence melting in the LTE during heating; whereas the main spherulitic structure melts during the HTE [1,2,16–18,20,27–29].

This dual melting behaviour is not observed in samples that undergo non-isothermal crystallisation. Crystallisation kinetics modelling shows that, during slow non-isothermal crystallisation where this dual melting behaviour is not observed, a dual crystallisation model is still necessary to obtain a good fit [20,30]. Some literature has highlighted the presence of a slight shoulder below the melting peak of PEEK after undergoing slow cooling, attributing it to the secondary crystallisation phase [23]. This shoulder is significantly less prominent than the distinct LTE observed after isothermal crystallisation and is absent during faster cooling rates. Such a shoulder is observable in some literature for higher PEKK grades [2] (higher crystallisation capability and faster kinetics), however, its nature is not discussed.

The impact of thermal history on the morphology has been studied on CF/PEEK, and more recently on CF/PEKK. Brittle fracture and matrix residue of CF/PEEK composites are present in slow-cooled [31] and isothermally crystallised [32] samples, indicative of high crystallinity content and a good fibre/matrix interface; whereas amorphous samples presented clean fibre surfaces and plastic yielding of the matrix [31,32]. Similar results were seen in a recent study on fractured CF/PEKK samples [20] after undergoing fast and slow cooling rates, as well as different spherulitic sizes as a consequence of isothermal hold in DSC cycles. Observations followed general nucleation theory, where at lower isothermal temperatures many, small spherulites were formed, and at higher temperatures, a lower number of spherulites but of larger dimensions could be seen.

While the above crystallisation studies are comprehensive, these have been performed with 5–20 mg of material in highly controlled, inert environments such as differential scanning calorimetry (DSC). Such conditions are unlikely to take place during manufacturing within an industrial context. It is therefore important to understand to what extent crystallinity influences mechanical performance under different manufacturing conditions. Studies correlating crystallinity with matrix-dominated properties of CF/PEEK overall show improved mechanical properties with a higher crystallinity [7,33,34], but as discussed in Pérez-Martín et al.'s review [3], diligent studies on the impact of thermal cycles on crystallinity and matrix performance are minimal. A study on the crystallinity and mechanical properties of CF/PEKK as a consequence of different processing methods has been recently published [35], however this does not evaluate the impact of varying individual process parameters on the crystallinity and performance. Outside of this, there are no studies correlating crystallinity with mechanical properties of CF/PEKK that the authors of this work are aware of. It is therefore of interest to understand how different processing conditions and resulting crystalline structures influence the performance of PEKK composites with high volume fraction of carbon fibres. This work compares the flexural 0 °, flexural 90 ° and interlaminar shear strength of unidirectional CF/PEKK laminates compression-moulded under different processing conditions and laminates manufactured by ATP. Laminates were also analysed via DSC and microscopy to obtain crystallinity levels and void contents, in order to establish the impact of different processing conditions on their mechanical performance and microstructure. Chemical etching was performed on the cross-section of some laminates to observe the impact of processing conditions on the developed crystal structures.

2. Materials and methods

2.1. Materials

In this study, laminates were produced using PEKK prepreg tapes unidirectionally reinforced with AS7 carbon fibres, provided by Hexcel Composites Ltd. The PEKK matrix is KEPSTAN PEKK 7002PT manufactured by Arkema. The polymer's glass transition temperature and melting temperature were measured at 160 °C and 337 °C respectively via DSC. The thickness of the prepreg tape was 0.2 mm. Two different rolls were used; one for compression moulding (150 mm wide prepreg roll), with a crystallinity of 18.2% and an average fibre volume fraction of 60.6% (measured via acid digestion); and one for ATP manufacturing (6.4 mm width prepreg tape), with a crystallinity of 19.2% and an average fibre volume fraction of 58.4%. For compression moulding, the prepreg roll was cut into 300 mm long prepreg sheets with a guillotine and stacked into layers.

2.2. Compression moulding

Unidirectional laminates were manufactured in a Pinette Emidecau Industries (PEI) LAB 450 P hydraulic press. Cooling of the press is provided by an integrated Frigosystem chiller. All laminates were made by stacking 10 plies of prepreg sheets with a layup $[0\ °]_{10}$ to achieve a thickness of 2 mm. A 3-part mould was used, consisting of a 2 mm-thick frame and a top and bottom plate, as shown in Fig. 1.

This resulted in laminates with dimensions 300 mm x 150 mm x 2 mm. Four laminates were manufactured undergoing the following

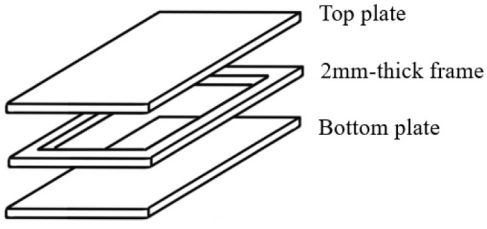

Fig. 1. Schematic of frame and plates used for compression-moulding manufacturing.

processing cycles. The selected isothermal and holding temperatures in the melt were chosen based on a previous study on the crystallisation behaviour and morphology of PEKK and CF/PEKK composites [20].

1. Heat from room temperature to holding temperature in the melt (370 °C or 380 °C) at 10 °C/min.
2. Hold in the melt for 25 min.
3. Cool down to isothermal temperature (220 °C, 260 °C or 300 °C) at 10 °C/min.
4. Hold at the isothermal temperature for 60 min.
5. Cool from the isothermal temperature to room temperature at 10 °C/min.

An additional laminate was manufactured undergoing a different processing cycle with no isothermal hold:

1. Heat from room temperature to holding temperature in the melt (370 °C) at 10 °C/min.
2. Hold in the melt for 25 min.
3. Cool from the melt temperature to room temperature at 5 °C/min.

A temperature-time plot of the described cycles is shown in Fig. 2. All laminates underwent a pressure of 1 bar during the heating step, and 28 bar for the remainder of the processing cycle. The laminates were named as shown in Fig. 2. The laminate code consists of three parts, denoting the nature of cooling ("I" for isothermal or "C" for dynamic cooling) followed by isothermal hold temperature (220 °C, 260 °C or 300 °C) or a cooling rate (5 °C/min), and finally the holding temperature in the melt (370 °C or 380 °C).

2.3. Automated Tape Placement (ATP)

Unidirectional ATP laminates were manufactured at the University of Limerick (Ireland) using a laser-assisted tape placement head (AFPT, GmbH) attached to a robot arm (Kuka, KR240 L210–2). A total of 10 layers of prepreg tape were placed per laminate, as per the compression-moulded laminates, resulting in 2 mm-thick laminates. A diagram of the process highlighting the ATP settings is shown in Fig. 3, and the names of the laminates with the parameters that were varied in this study are given in Table 1. The laminate code consists of the nip temperature (370, 380 or 390 °C), lay-down speed (2 or 4 m/min) and roller pressure (2 or 4 bar). Comparisons in laminate properties and performance have been drawn across these three parameters in Section 3.

In this work, the tool on which the laminates were manufactured was unheated and made out of mild steel, and a repass on the final layer of each laminate was done. Repasses are often performed to improve interply consolidation, crystallinity and hence mechanical performance of the part [12].

While in this work it is not possible to assess the cooling rates that the tape undergoes during lay-down, previous literature [15] has reported steep temperature drops in CF/PEKK tapes when manufactured on an unheated tool using ATP. Using a laser source, cooling rates between 150 and 220 °C/min were achieved in the first second of cooling, the rates being higher on the first layers of prepreg tape that were laid on the unheated surface of the tool.

2.4. Microscopy

Void content was calculated using optical microscopy images taken with a Leica DM6000 M microscope after casting, grinding and polishing the laminate samples. These images were then analysed with ImageJ software, using the threshold tool to calculate void content area. This calculates the area that pixels above or below a certain threshold value take up of the image being analysed. An example of how this was done is shown in Fig. 4. Void content was taken from images that encompassed the entire thickness of a laminate cross-section ignoring defects close to the laminate surfaces (6 images per laminate). The total evaluated area per laminate was approximately 1250 μm x 1400 μm.

2.5. Differential scanning calorimetry (DSC)

Crystallinity measurements were obtained by cutting three samples from randomly selected locations of each laminate. Scans at dynamic heating rates of 20 °C/min from room temperature to 370 °C were carried out using a Mettler Toledo DSC 3 + , with aluminium pans non-hermetically sealed with aluminium lids. Sample masses of 10–20 mg were used. All experiments were performed under a nitrogen environment to avoid any sample degradation.

The crystallinity of a sample was estimated with:

$$\chi = \frac{\Delta H_m - \Delta H_{cc}}{\alpha \times \Delta H_{100\%}} \quad (1)$$

where ΔH_m is the melting enthalpy, ΔH_{cc} is the cold crystallisation enthalpy, α is the weight fraction of matrix content (31.7% for the compression moulding tape and 34.5% for the ATP tape) and $\Delta H_{100\%}$ is the theoretical melting enthalpy of 100% crystalline PEKK. This has been calculated to be 130 J/g by Chang and Hsiao [15].

2.6. Chemical etching

Chemical etching was performed on laminates I-220–370, I-260–370 and I-300–370 to observe the impact of isothermal temperature on the matrix morphology. Cross-section samples of the laminates were cast in

Compression-moulded laminates

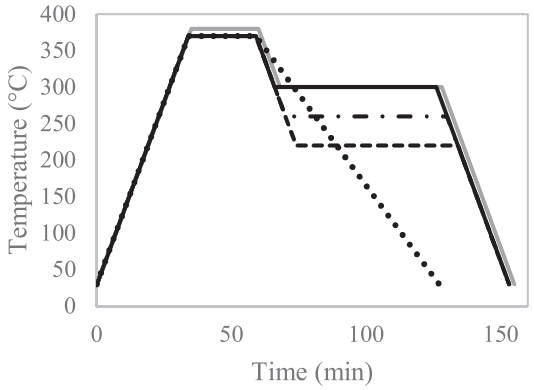

Legend	Laminate code	Hold melt temp. (°C)	Isothermal hold temp. (°C)
- - -	I-220-370	370	220
— · ·	I-260-370	370	260
———	I-300-370	370	300
———	I-300-380	380	300

Legend	Laminate number	Hold melt temp. (°C)	Cooling rate (°C/min)
▪▪▪▪	C-5-370	370	5

Fig. 2. Summary of processing parameters for the compression-moulded laminates.

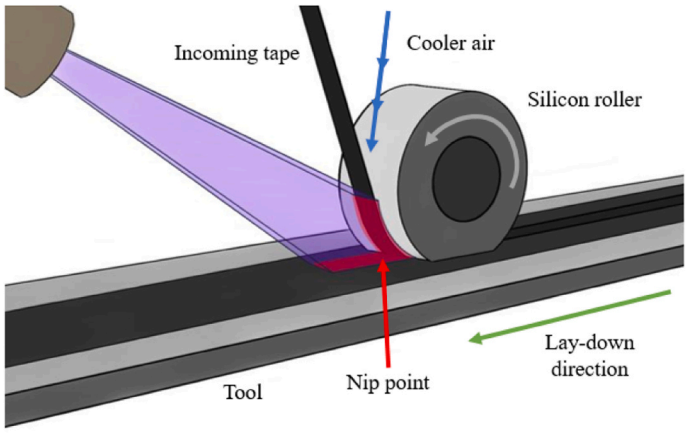

Cooler air pressure	1 bar
Incoming tape dimensions	6.4mm wide x 0.2mm thick
Laser-nip point optical distance	170mm
Laser power limit	1000W
Tape/laminate laser split	Approx. 50/50
Tool temperature	Unheated

Fig. 3. Schematic of ATP lay-up process and processing parameters. ATP schematic drawn after [5].

Table 1
Summary of processing parameters for the ATP-manufactured laminates.

Laminate code	Nip temperature (°C)	Lay-down speed (m/min)	Roller pressure (bar)
370–4–2	370	4	2
380–4–2	380	4	2
390–4–2	390	4	2
380–2–2	380	2	2
380–4–4	380	4	4

epoxy resin, and polished with silicon carbide discs of grits up to P2500, followed by diamond suspensions of down to 1 μm particle size. These were then etched following the steps below, based on the etching methods reported in literature for CF/PEEK, where spherulitic structures have been successfully observed [22,36]:

1. Immerse in a stirred solution of 1% potassium permanganate in a 5:2:2 solution of sulphuric acid, orthophosphoric acid and distilled water. Constant stirring was provided by a magnetic stirrer at approximately 100 rpm.
2. Carefully wash in a 7:2 solution of sulphuric acid and distilled water.
3. Wash in 30% hydrogen peroxide solution.
4. Wash in distilled water.

This procedure was performed twice. The first time, steps 1 and 2 were carried out for 7 and 3 min respectively; the second time they were carried out for 10 and 5 min respectively.

2.7. Mechanical testing

2.7.1. Flexural testing

0 ° and 90 ° flexural testing were performed in accordance with ASTM D7264, using a span-to-thickness ratio of 32:1 and a specimen length about 20% longer than the support span. This resulted in coupon dimensions of 80 mm x 13 mm, and a span of 64 mm. Eight coupons were tested per laminate in each orientation. A crosshead speed of 3 mm/min was used until failure on an Instron 3369 testing system.

2.7.2. Short beam shear testing (interlaminar shear strength)

Interlaminar shear performance was assessed in accordance with ASTM D2344, using a span-to-thickness ratio of 4:1, a length-to-thickness ratio of 6:1 and a width-to-thickness ratio of 2:1. Eight coupons were tested per laminate. Coupon dimensions were therefore 12 mm x 4 mm, with a span of 8 mm. Testing was performed at 1 mm/min on an Instron 3369 testing system.

2.8. Scanning electron microscopy (SEM)

SEM was performed on post-mortem flexural and ILSS coupons in order to qualitatively assess failure behaviour. Flexural coupons were cut down to a size that allowed for SEM observation of the fracture area, taking care to not affect the region of interest. ILSS coupons were cast exposing the edges of the samples and polished. SEM was also performed on the aforementioned etched samples, in order to observe differences in the crystalline structures. Samples were prepared with a 15 nm sputter coating of gold to enhance surface conductivity and imaged with a JEOL

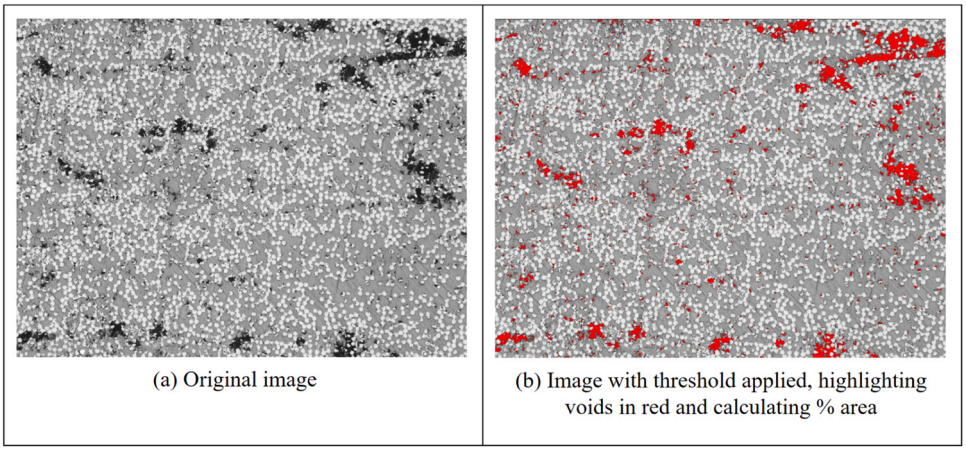

Fig. 4. Sample image from ATP laminate 380–4–2 (a) original image (b) after applying the threshold tool on ImageJ.

JSM-IT100 instrument at 20 kV.

3. Results and discussion

The manufactured laminates were examined for their consolidation quality and crystalline morphology, and were tested for flexural (longitudinal and transverse) and interlaminar shear strength properties. The following sections discuss the results of these tests.

3.1. Laminate consolidation

Fig. 5 shows sample microscopy images of mounted and polished compression-moulded and ATP samples, where fibre, matrix and any voids present can be observed. Table 2 shows the average thickness and per cent void content for each laminate taken from Fig. 5.

Overall, no significant variability was observed in the thickness or void content across the compression-moulded laminates. Although the thermal history of each laminate is different, these were held in the melt and at the isothermal temperatures for long times (60 min) under high pressure (28 bar), and therefore a low void content was expected. This processing, along with the frame used, limited the laminate thickness of the compression-moulded laminates to the thickness of the frame, explaining the low variability in thickness across the different laminates. The different prepreg layers are still distinguishable in the micrographs of all the laminates.

On the other hand, the ATP laminates showed a significantly higher void content. This is a consequence of the much shorter exposure time to high temperatures and pressures which limit flow of the matrix into voids and the extent of interply contact, evident in the interply voids highlighted with blue squares in Fig. 5. Intraply voids (highlighted with red arrows) are also present, which could be attributed to the inadequate penetration of the matrix into the fibres in the prepreg tape. The pressure during compression moulding is high enough to minimise these, but not during the ATP lay-down process. Other authors have made similar

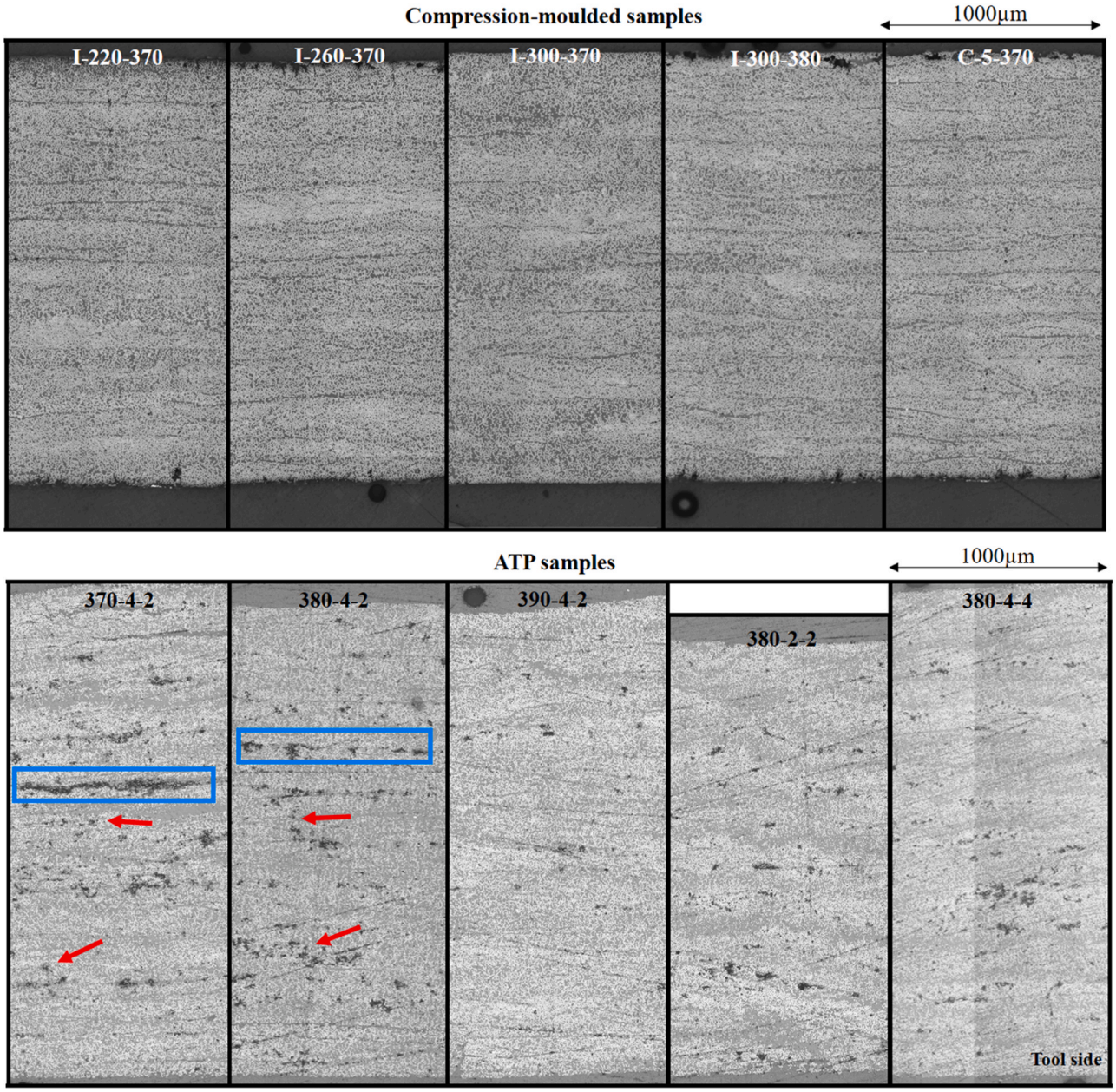

Fig. 5. Microscopy images of the cross sections of all compression-moulded laminates and the ATP-manufactured laminates with annotations highlighting examples of interply voids (blue squares) and intraply voids (red arrows).

Table 2
Laminate thickness and void content of compression-moulded and ATP laminates, taken from microscopy images in Fig. 5.

	Laminate	Laminate thickness (mm)	Void content (%)
Compression-moulded	I-220–370	1.92 ± 0.00	0.4 ± 0.2
	I-260–370	1.89 ± 0.01	0.1 ± 0.1
	I-300–370	1.93 ± 0.00	0.1 ± 0.1
	I-300–380	1.92 ± 0.01	0.2 ± 0.0
	C-5–370	1.91 ± 0.01	0.4 ± 0.1
ATP	370–4–2	2.20 ± 0.03	7.9 ± 2.7
	380–4–2	2.13 ± 0.01	8.0 ± 1.1
	390–4–2	2.11 ± 0.03	3.7 ± 0.5
	380–2–2	1.95 ± 0.02	6.0 ± 0.5
	380–4–4	2.24 ± 0.02	5.7 ± 1.8

observations when comparing CF/PEEK ATP-manufactured laminates with autoclaved laminates. For example, in Comer et al.'s work [6], void content was measured at 2.83% and 0.08% in ATP and autoclaved laminates respectively. They also cited other works on ATP-manufactured CF/PEEK laminates [37–39] where void content varied from 1.65% to 7%, in line with the observations in this study. Qureshi et al. [10] also drew qualitative comparisons between microscopy images of autoclaved and ATP CF/PEEK laminates where the higher void content in the ATP-manufactured laminates was evident.

The effect of the lower pressure applied for shorter times also became obvious when comparing the ATP laminate thicknesses with that of the compression moulded laminates: with the same number of plies, thicknesses were 1.89–1.93 mm for the compression-moulded laminates and 1.95–2.24 mm for the ATP laminates.

Some differences, albeit less significant, can also be observed across the different ATP laminates. A slower lay-down speed resulted in a thinner laminate, less defined interply boundaries and a lower void content, visible when comparing laminates 380–4–2 and 380–2–2. Roller pressure may have also impacted the presence of voids: interply voids appear more localised in 380–4–4, whereas in 380–4–2 they seem more elongated and distributed along interply boundaries.

Higher nip temperatures clearly caused a decrease in void content, particularly noticeable in Fig. 5 when comparing 370–4–2 and 390–4–2. A higher temperature likely resulted in the polymer being held at a lower viscous state for longer, resulting in better interply adhesion. Consequently, the thickness also decreased with a higher nip temperature, but the drop is less significant.

3.2. Crystallinity and spherulitic morphology

Table 3 shows the average glass transition temperatures, enthalpies and total crystallinities achieved in the manufactured laminates, with Fig. 6 showing heat flow variation against temperature in DSC for one sample of each laminate. All the compression-moulded laminates crystallised to the maximum extent (~29%), whereas the ATP-manufactured laminates only achieved 6–8.3% crystallinity and contained a significant amorphous fraction. This amorphous content is denoted by the cold crystallisation peak and the much more prominent glass transition in the ATP sample curves in Fig. 6.

The melting behaviour of the isothermally compression-moulded laminates in DSC denote a dual crystallisation mechanism previously observed for both PEEK and PEKK systems[1–3,17,20,22,24,27,40,41]. The LTEs (marked * in Fig. 6) are observed to shift, depending on the isothermal temperature (T_{iso}) the material underwent, always remaining approximately 10 °C above T_{iso}. The proportion of LTE:HTE also increased with T_{iso}, as observed in a previous study performed on the same prepreg tape undergoing different cycles in DSC [20]. The proportion of HTE is higher in the current study, which may be a consequence of the slower cooling rate the material undergoes to reach T_{iso} (10 °C/min instead of 150 °C/min used in DSC), as well as the sample size: the laminates consist of 10 layers of prepreg tape across which heat flow may be slower than the small prepreg sample used in the previous DSC studies. During non-isothermal processing (as per laminate C-5–370), PEKK does not display this dual melting behaviour, but rather a single melting peak (corresponding to the HTE in the isothermal laminates).

In the case of laminates I-300–370 and I-300–380, where the holding temperatures in the melt were 370 °C and 380 °C respectively and isothermal hold temperature was 300 °C, both endotherms in Fig. 6 (LTE and HTE) began to overlap, as observed in previous studies [2,17,20]. In this case, the area corresponding to each endotherm was calculated as done in [20]. There is no significant difference observed as a consequence of the different holding temperatures in the melt.

The ATP-manufactured laminates, on the other hand, achieved a

Table 3
Average values for glass transition temperatures, enthalpies and total crystallinity of CF/PEKK laminates manufactured under different processing conditions.

	Laminate	T_g (°C)	T_{LTE} (°C)	ΔH_{LTE} (J/g)	T_{HTE} (°C)	ΔH_{HTE} (J/g)	LTE:HTE	X (%)
Compression-moulded	I-220–370	155.5 ± 1.4	231.6 ± 0.5	0.27 ± 0.01	341.3 ± 0.6	11.8 ± 0.6	2:98 ± 0	29.3 ± 1.4
	I-260–370	157.0 ± 3.2	271.0 ± 0.7	0.38 ± 0.03	340.8 ± 0.6	10.7 ± 0.4	3:97 ± 0	27.0 ± 1.0
	I-300–370	156.6 ± 205	309.9 ± 0.2	2.9 ± 0.2	341.4 ± 0.8	9.1 ± 0.5	24:76 ± 1	29.1 ± 1.3
	I-300–380	160.2 ± 0.4	306.6 ± 0.1	2.9 ± 0.2	340.9 ± 0.7	10.0 ± 0.4	22:78 ± 1	31.2 ± 0.4
	C-5–370	151.9 ± 0.8	-	-	341.7 ± 1.1	11.7 ± 0.2	-	28.5 ± 0.4
ATP		**T_g (°C)**	**T_{cc} (°C)**	**ΔH_{cc} (J/g)**	**T_m (°C)**	**ΔH_m (J/g)**	**-**	**X (%)**
	370–4–2	162.6 ± 1.0	220.5 ± 0.3	9.0 ± 0.5	337.8 ± 1.3	11.7 ± 0.7	-	6.0 ± 0.5
	380–4–2	165.3 ± 4.1	220.2 ± 3.8	9.1 ± 0.3	339.2 ± 2.7	12.5 ± 0.5	-	6.8 ± 1.3
	390–4–2	164.7 ± 0.4	223.5 ± 2.6	9.0 ± 1.0	339.2 ± 0.4	11.8 ± 1.0	-	6.1 ± 0.5
	380–2–2	162.6 ± 0.3	217.8 ± 0.4	8.6 ± 0.2	338.2 ± 0.6	12.5 ± 0.9	-	8.3 ± 1.0
	380–4–4	163.8 ± 2.1	220.5 ± 1.3	9.0 ± 0.1	338.4 ± 1.7	11.7 ± 0.7	-	6.0 ± 1.6

T_g = glass transition temperature
T_{LTE} = low endotherm temperature
ΔH_{LTE} = low endotherm enthalpy
T_{HTE} = high endotherm temperature
ΔH_{HTE} = high endotherm enthalpy
LTE:HTE = low endotherm to high endotherm ratio
X = total crystallinity
T_{cc} = cold crystallisation temperature
ΔH_{cc} = cold crystallisation enthalpy
T_m = melting temperature
ΔH_m = melting enthalpy

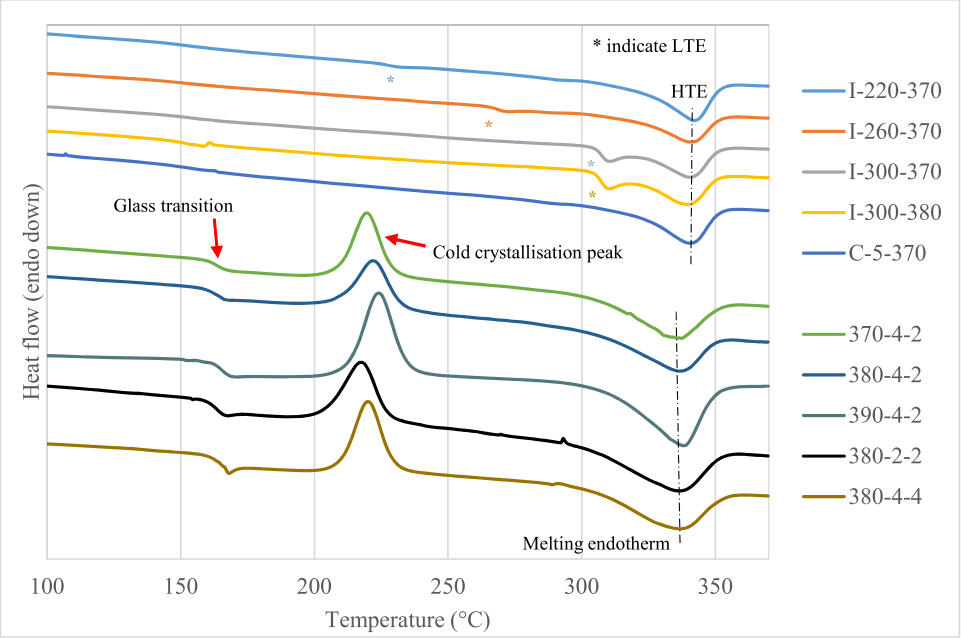

Fig. 6. Sample DSC heat scans of CF/PEKK laminates manufactured under different processing conditions.

lower crystallinity than what the prepreg tape originally contained, and did not show any form of dual melting behaviour in the DSC heat scan. This may be attributed to the slower crystallisation kinetics of PEKK compared to PEEK [3] and the short time that the matrix is exposed to temperatures at which it can undergo crystallisation, developing a limited amount of primary crystallisation and no secondary crystallisation phase due to its slower forming nature. This is further evidenced by the cold crystallisation peak that takes place during heating (Fig. 6), showing that the matrix did not fully crystallise during processing. Laminate 380–2–2, with a slower lay-down speed of 2 m/min, achieved a slightly higher crystallisation, likely due to this lower speed resulting in longer exposure times of the material to temperatures within crystallisation range (between glass transition temperature and melting temperature). Nip temperature and roller pressure did not seem to have an effect on the crystallisation extent.

Fig. 7a, b and c show etched samples from laminates I-220–370, I-

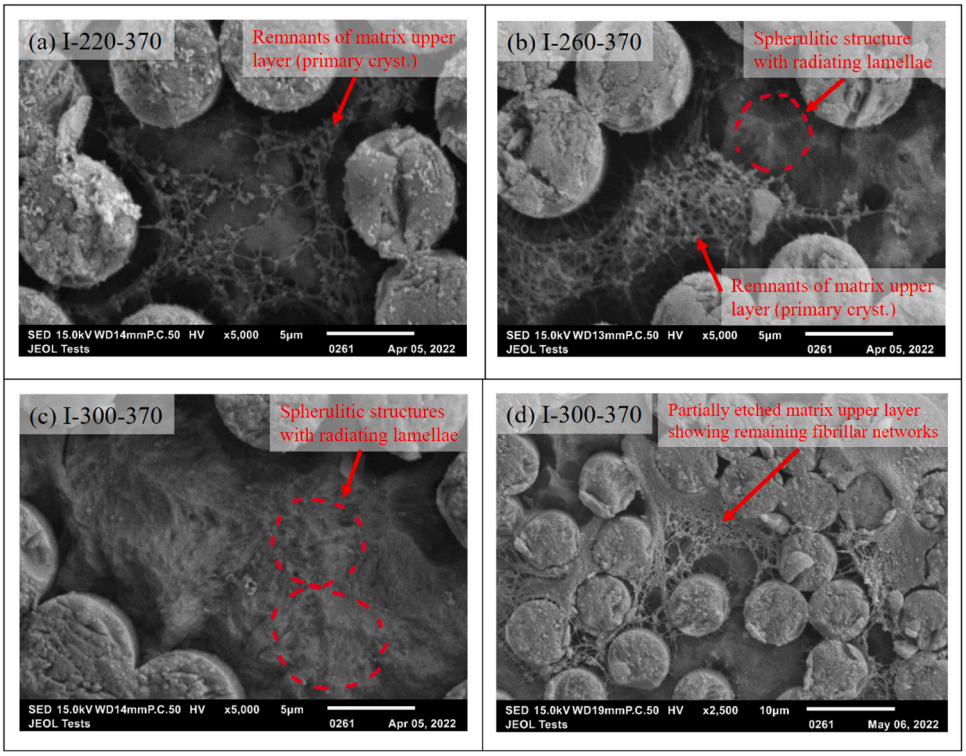

Fig. 7. SEM micrographs of etched CF/PEKK samples from different compression-moulded laminates: (a) Laminate I-220–270 (b) Laminate I-260–370 and (c) Laminate I-300–370 (d) example of partially etched sample showing remaining fibrillar networks in the matrix as a consequence of partial etching.

260–370 and I-300–370 respectively. These samples were selected to observe the effect of different isothermal holding temperatures on the developed matrix morphology. Fig. 7d shows a partially etched sample, where the top layer of the matrix has not been fully etched. Here the fibrillar networks in the matrix can be observed to be the last to remain from the top matrix layer as the etchant exposes the lower layer of the matrix. These networks are likely to be remnants of the primary crystal structure of the matrix, with amorphous material being etched first, followed by secondary crystals, and finally the primary crystalline structures.

Across all images in Fig. 7 it is obvious that the fibre-matrix interface region was more severely impacted by the etching than the bulk matrix. This suggests a fibre-matrix interface with a lower chemical resistance than the matrix bulk. This could be due to the presence of a trans-crystalline region with lower chemical resistance.

In the bulk matrix of the samples in Fig. 7b and c, the preferential etching of the amorphous regions revealed radiating patterns typical of spherulitic crystallisation. The spherulite size is larger in Fig. 7c where the sample was held at the higher isotherm (300 °C), a consequence of the lower nucleation density at higher isothermal temperatures. The spherulite sizes are therefore expected to be the smallest in Fig. 7a with the highest nucleation density out of the three samples. These are not particularly obvious potentially due to spherulites being very small, as well as the network-like structure present over the etched surface in Fig. 7a. While these network structures were present in all samples, these were observed the most in the etched sample of laminate I-220–370 and I-260–370, and the least in the laminate I-300–370. From the DSC results shown in Fig. 6 and Table 3, there is a larger proportion of material that melts under the HTE in samples undergoing lower T_{iso}, and therefore a larger proportion of the more stable primary crystalline structure. It is therefore logical that there is more of this residual primary structure present in Fig. 7a, and the least in Fig. 7c.

Similar conclusions on the variation of spherulite size have been observed in literature. As discussed in Section 1, a preceding study [20] observed cryofractured CF/PEKK samples undergoing isothermal holds in DSC cycles to develop small spherulites at lower isothermal temperatures, and larger spherulites at higher isothermal holds. Other work on CF/PEEK also observed such behaviour [36].

3.3. Mechanical performance

The results of the mechanical testing are discussed in this section. Overall, there was no significant difference in the performance of the different compression-moulded laminates, except for a marginally improved performance of Laminate I-300–380 in Flexural 90°. On the other hand, lower properties were observed in the ATP-manufactured laminates across all tests. A summary of all mechanical testing results is presented in Table 4, and will be discussed in detail in the following sub-sections. Mechanical testing data reported in literature for ATP-manufactured CF/PEKK (AS7 fibres as used in this study) laminates is scarce, and therefore available results on CF/PEEK with different fibre types (AS4, IM7) are also included for comparative purposes.

3.3.1. Flexural 0 ° (longitudinal) testing

Representative flexural 0 ° stress-strain curves for each laminate are shown in Fig. 8. Coupon failure in this testing mode commenced by compression on the top surface of the specimens (where the load was being applied), followed by tension failure on the bottom surface. While flexural 0 ° testing response is dominated by the fibres, the matrix also plays a role in providing compression strength in particular, and therefore may influence flexural properties to some extent.

No significant difference in flexural strength or modulus was observed across the different compression-moulded laminates, implying that differences in the crystal morphology, as a consequence of the differing isothermal holds or holding temperatures in the melt, have not resulted in significant differences in the behaviour of the matrix when loaded under 0 ° flexure. This was expected, as longitudinal flexural testing is dominated by fibre strength rather than the matrix. The failure of the composites was also abrupt and explosive, with the majority of the samples splitting in two when reaching the maximum load. It is obvious, however, that processing conditions did have an effect on flexural 0 ° performance to a certain extent, as shown by the lower flexural strength and modulus of the ATP specimens by 62% and 25% respectively on average. The higher void content is likely to lead to lower mechanical properties; as well as the amorphous nature of the matrix in the ATP specimens resulting in a more ductile behaviour. This therefore resulted in sample deformation and failure under lower loads than the compression-moulded specimens. This more plastic behaviour is also reflected in the fact that, unlike the compression-moulded specimens, the ATP flexural specimens did not experience an explosive fracture nor completely split into two. Instead, a jagged fracture curve was observed in Fig. 8, indicating that the ATP samples failed in various steps. This is due to the poorer consolidation of the laminates observed in Section 3.1, which resulted in different groups of plies failing at different stages. This is visible in the SEM images of the fracture surfaces shown in Fig. 9 – in the compression-moulded sample, single compression and tension regions are visible, whereas in the ATP sample these can be seen to alternate, indicating several steps to failure.

Comparing the results in Table 4 for the different ATP laminates, it is obvious that higher nip temperatures (380 and 390 °C) increase 0 ° flexural performance, particularly flexural strength, possibly a consequence of achieving a better interlayer adhesion during material lay-down. A slower lay-down speed likely had the same impact, marginally increasing the performance of laminate 380–2–2 compared to laminate 380–4–2. This may have also been influenced by the slightly higher crystallinity content resulting from a slower lay-down speed. Laminate 380–4–4, with a higher roller pressure, did not show any significant difference, potentially indicating that at this nip temperature and lay-down speed, increasing roller pressure does not have an impact on laminate consolidation.

Higher magnification SEM images of the fracture surfaces of a compression-moulded specimen and an ATP specimen are shown in

Table 4
Mechanical testing results of compression-moulded and ATP CF/PEKK laminates.

	Laminate	Flexural 0°		Flexural 90°		ILSS
		Strength (MPa)	Modulus (GPa)	Strength (MPa)	Modulus (GPa)	SBS Strength (MPa)
Compression-moulded	I-220–370	1824 ± 119	120.1 ± 1.7	75.5 ± 2.0	8.6 ± 0.2	97.9 ± 0.5
	I-260–370	1825 ± 135	120.6 ± 2.6	75.8 ± 3.0	8.6 ± 0.2	97.9 ± 1.8
	I-300–370	1770 ± 107	120.1 ± 1.7	77.6 ± 7.3	8.6 ± 0.2	99.4 ± 3.0
	I-300–380	1772 ± 95	119.2 ± 2.5	93.9 ± 7.0	8.6 ± 0.2	100.1 ± 3.1
	C-5–370	1855 ± 64	121.2 ± 2.0	81.0 ± 3.5	8.7 ± 0.1	93.0 ± 4.6
ATP	370–4–2	457.8 ± 35.8	88.8 ± 7.4	20.8 ± 4.9	2.2 ± 0.6	22.0 ± 1.6
	380–4–2	718.8 ± 73.1	95.8 ± 2.8	31.3 ± 2.3	3.4 ± 0.3	24.4 ± 2.0
	390–4–2	755.7 ± 58.9	91.9 ± 6.1	27.1 ± 4.4	2.6 ± 0.5	29.3 ± 1.7
	380–2–2	761.0 ± 50.1	87.1 ± 4.8	24.1 ± 2.1	2.9 ± 0.6	27.0 ± 2.4
	380–4–4	741.7 ± 98.9	86.9 ± 8.7	24.1 ± 1.6	3.1 ± 0.2	26.6 ± 2.0

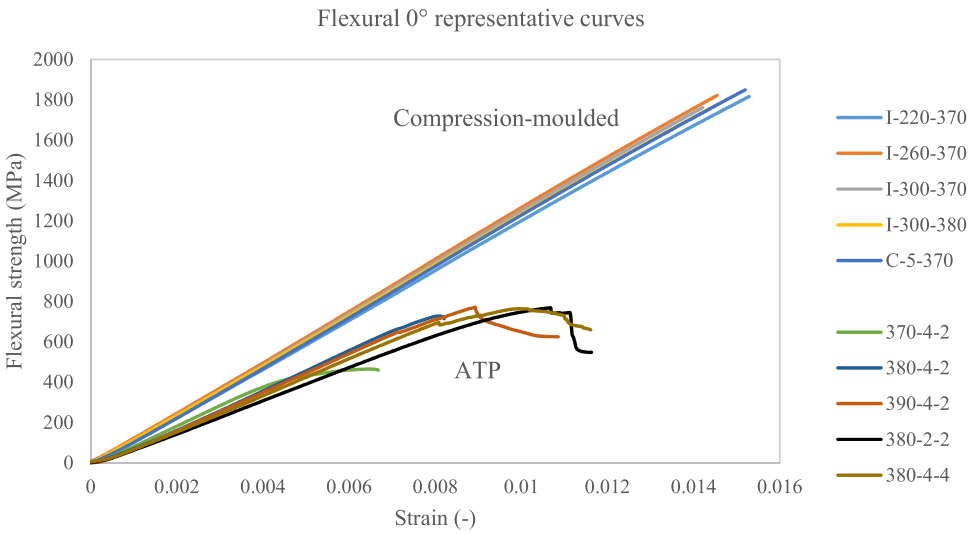

Fig. 8. Representative stress-strain curves for flexural 0° coupons of compression-moulded and ATP laminates.

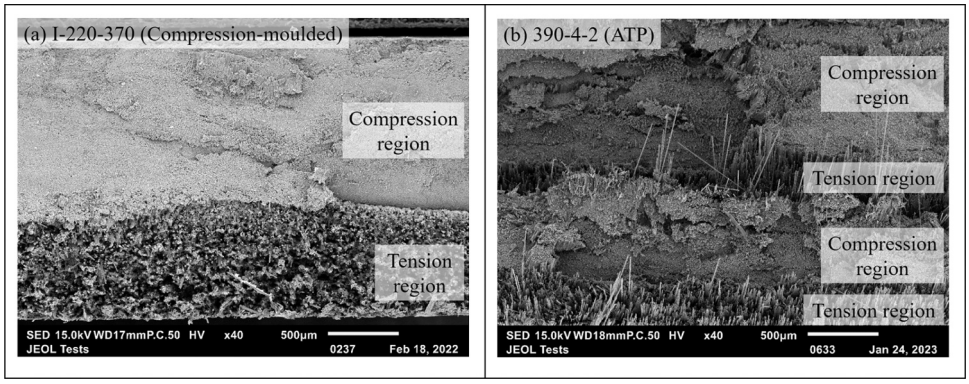

Fig. 9. SEM images of 0 ° flexural fracture surfaces of specimens extracted from (a) I-220–370 (compression moulded) and (b) 390–4–2 (ATP-manufactured) laminates at × 40 magnification, with labelled tension and compression failure regions.

Fig. 10. Across all compression-moulded specimens, fibre surfaces were observed to be coated with matrix, with no major differences across the different samples, whereas the ATP specimens showed bare fibres. This suggests that the processing conditions influenced the fibre-matrix interface, with a higher crystallinity resulting in better adhesion of the matrix to the fibre surface. As mentioned in Section 1, this is in line with what has previously been observed in literature, with high crystallinity content in CF/PEEK [31,32] and CF/PEKK [20] fracture samples displaying a significant amount of matrix residue on fibres, whereas amorphous samples resulted in clean fibre surfaces.

A comparison of the above results of CF/PEKK with results from the literature on CF/PEEK is given in Table 5. The compression-moulded CF/PEKK samples performed comparably to autoclaved CF/PEEK samples, whereas the ATP laminates tested in this work underperformed in comparison to reported CF/PEEK values. This may be a consequence of the ATP process parameters selected in the current study limiting interply consolidation and resulting in higher void content, as discussed in Section 3.1.

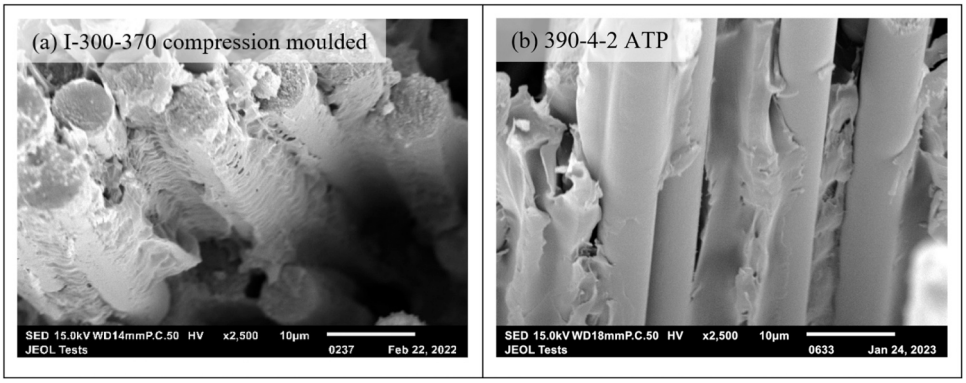

Fig. 10. SEM images of 0 ° flexural fracture surfaces of specimens extracted from (a) I-300–370 (compression moulded) and (b) 390–4–2 (ATP).

Table 5
Flexural 0 ° results in this work and in literature.

Material [Ref]	Autoclave	Laser ATP					
	Flexural 0 ° (MPa)	Nip temp. (°C)	Tool temp. (°C)	Tool material	Lay-down speed (m/min)	Roller pressure (bar)	Flexural 0 ° Strength (MPa)
AS4/PEEK[42]	1650	420	Unheated	Stainless steel	9	3.8	1143
AS4/PPS/PEEK[42]	1650	400	Unheated	Stainless steel	9	3.8	1035
This work, AS7/PEKK	1770–1855 (comp. moulding)	370	Unheated	Mild steel	4	2	457.8
		380	Unheated	Mild steel	4	2	718.8
		390	Unheated	Mild steel	4	2	755.7
		380	Unheated	Mild steel	2	2	761.0
		380	Unheated	Mild steel	4	4	741.7

3.3.2. *Flexural 90 ° (transverse) testing*

Representative flexural 90 ° stress-strain curves for each laminate are shown in Fig. 11. In this testing mode, failure was caused purely by tension, which began on the bottom surface of the samples (side under tension). Fibre contribution to strength and stiffness is minimal in this case, and therefore this test can provide a better indication of any variation in matrix properties as a consequence of processing.

There was a significant increase of approximately 23% in the 90 ° flexural strength of laminate I-300–380 compared to the remaining compression-moulded laminates, which showed no significant difference in performance. This suggests that a different crystalline morphology as a consequence of different isothermal holds (large vs. small spherulites) does not majorly dictate flexural performance when loaded under 90° flexure as long as the material is crystallised to its maximum extent (~29%). The crystallinity of laminate I-300–380 (shown in Table 3) was also the highest, which may contribute to the better performance. All compression-moulded samples exhibited immediate load drop after reaching the peak load.

The ATP specimens showed significantly lower flexural strength and modulus (~68% and 67% respectively) compared to the compression-moulded laminates. The more amorphous nature of the matrix resulted in lower material strength and stiffness, as mentioned before. The higher ductility in the material is once again apparent in the representative curves in Fig. 11, where the load did not immediately drop after failure. The ATP laminates manufactured with higher nip temperatures (380 and 390 °C) performed best, indicating that higher processing temperatures contributed towards a better performance. This may be a consequence of the lower void content and an overall better consolidation as observed in the laminate thickness in Section 3.1. A slower lay-down speed and a higher roller pressure did not seem to have a significant impact on changing matrix flexural strength in this case.

SEM images of the 90 ° flexural fracture surfaces of compression-moulded and ATP specimens in Fig. 12 show coated fibres in the compression-moulded specimen, and clean fibres in the ATP sample. Similarly to 0 ° flexural fracture images, this suggests a weak fibre-matrix interface with an amorphous matrix in the ATP specimen, causing failure at said interface rather than in the matrix bulk.

Comparing the flexural 90 ° results to literature, the compression-moulded CF/PEKK laminates in this study (75–94 MPa) performed comparably with CF/PEEK laminates manufactured via autoclave (~90 MPa [8]) and compression moulding (55–130 MPa [7,43]). Literature covering flexural 90 ° testing of ATP-manufactured CF/PEEK or CF/PEKK laminates has not been found.

3.3.3. *Interlaminar shear strength (ILSS)*

Representative stress-displacement curves from the ILSS tests are shown in Fig. 13. No significant variation in performance was observed across the isothermally compression-moulded laminates, with a marginally lower performance in the ILSS of dynamically cooled laminate C-5–370 (−6%). As this laminate underwent non-isothermal cooling at a rate of 5 °C/min, there was a steady decrease in the matrix molecular movement with the drop in temperature as the material cooled down. The laminate was also exposed to temperatures in which interply consolidation could happen above glass transition temperature for a shorter time than the rest of the compression-moulded laminates. This is visible in Fig. 1, where the temperature in laminate C-5–370 dropped below 160 °C (T_g) after 100 min, whereas the rest of the compression-moulded laminates dropped below 160 °C after approximately 140 min. Therefore, it is possible that a slower cooling rate, particularly at the temperature range where a better interply consolidation can be achieved (above T_g), might improve this result. However, if the difference in performance is marginal between laminates

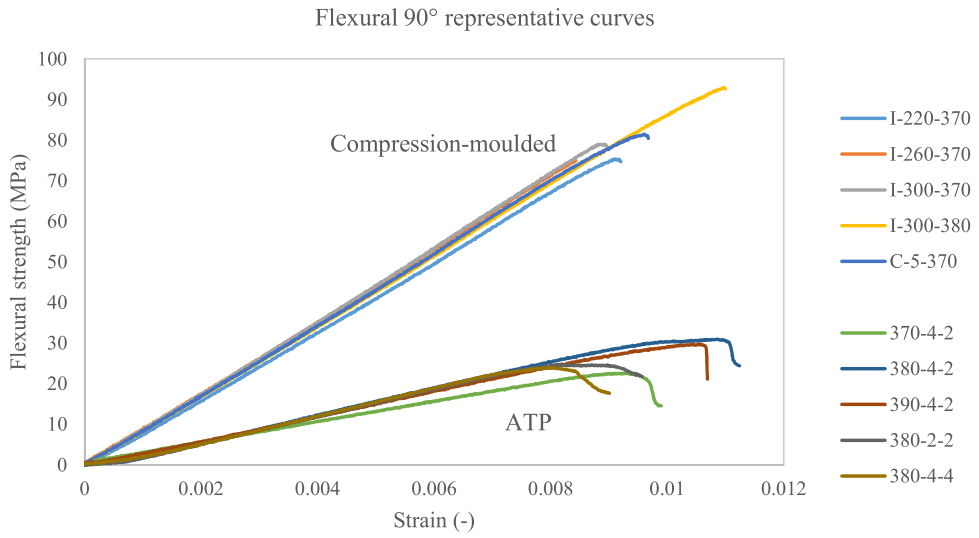

Fig. 11. Representative stress-strain curves for flexural 90 ° coupons of compression-moulded and ATP laminates.

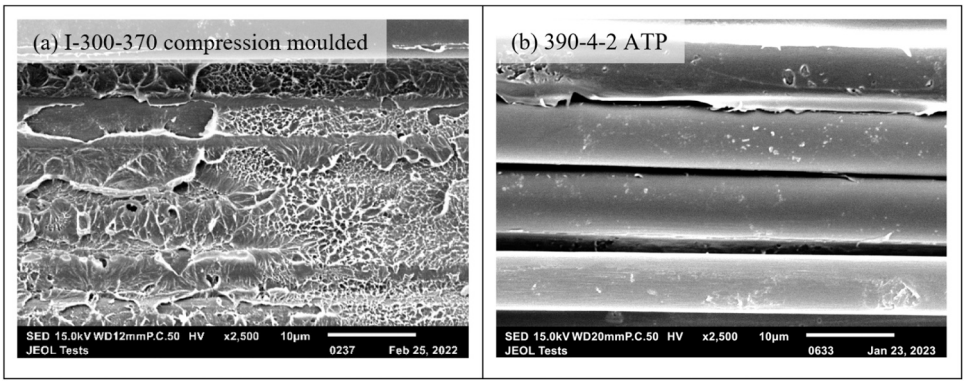

Fig. 12. SEM images of 90 ° flexural fracture surfaces of specimens extracted from (a) I-300–370 (compression moulded) and (b) 390–4–2 (ATP).

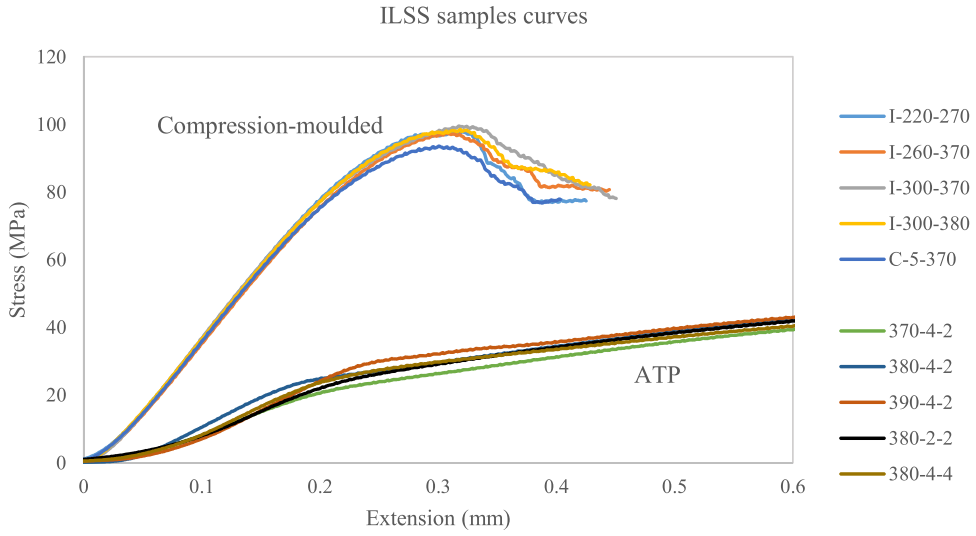

Fig. 13. Representative ILSS stress-displacement curves of compression-moulded and ATP laminates.

undergoing a slower cooling rate or undergoing an isothermal hold at a higher temperature for a definite period of time, then the more energy-efficient cycle should be considered in large-scale manufacturing.

The ATP laminate specimens, on the other hand, exhibited 73% lower ILSS compared to the compression-moulded laminates. This is very likely due to the much shorter exposure times to heat and pressure experienced during manufacturing, which resulted in a higher void content and lower interply consolidation than that achieved by compression moulding. It can also be observed in Fig. 13 that the response of the ATP specimens was unlike the other specimens and not what is commonly seen in an ILSS load-displacement curve (no ILSS peak). Instead, they displayed much more plastic deformation after the initial linear portion of the graph. Similar behaviour was observed in Chanteli et al.'s work on CF/PEEK [12], where the influence of repass on laser-ATP-manufactured laminates was studied, and no distinct peak was observed in their load-displacement curves. In this case, the authors argued that the non-linear response was a consequence of the visco-elastic behaviour of the matrix. Comer et al. [6] observed a slightly more defined curvature in the fail response of laser-ATP manufactured CF/PEEK, potentially due to the faster crystallising nature of PEEK compared to PEKK; however performance compared to autoclaved samples was still significantly lower.

As with the previous testing, the ILSS performance of the laminates can be observed to marginally increase with a higher nip temperature, again potentially indicating a better interlayer adhesion. As per the 0 ° flexural testing, there was also a marginal increase in ILSS with a slower lay-down speed (380−2−2) and a higher roller pressure (380−4−4) when compared to 380–4–2. This is likely due to the better consolidation reflected in the lower void content observed in Section 3.1.

The difference in performance between compression-moulded and ATP ILSS coupons becomes obvious in the SEM images shown in Fig. 14. The compression-moulded laminates showed a kink in the fibres under the location of the loading nose (flexural failure by compression) and/or ply separation (interlaminar shear) (Fig. 14a). On the other hand, the ATP specimens did not show either of these features, and instead displayed inelastic deformation (Fig. 14b). The voids visible in Fig. 14b(iv) have also been observed in untested specimens to a lesser extent (see Fig. 15). It is possible that the voids already present in the untested samples were exacerbated during ILSS testing, specifically those present between plies (particularly obvious in Fig. 14b(iv)). This is the case in Chanteli et al.'s work [12], where side-images of ILSS coupons from CF/PEEK ATP laminates show some elongated voids from interlayer separation/delamination and no brittle deformation as per the compression-moulded laminates in this work.

A comparison of ILSS results of CF/PEKK with that of CF/PEEK in literature, as well as a recent study on CF/PEKK, is given in Table 6. The compression-moulded laminates in our work performed similarly to the autoclaved CF/PEEK [12] and CF/PEKK [35] laminates reported in literature. This was also the case for the ATP laminates when compared to published work with similar nip temperatures and an unheated tool, showing a significant drop of 57% for CF/PEEK [12] and 77% for CF/PEKK [35] when compared to their respective autoclaved results.

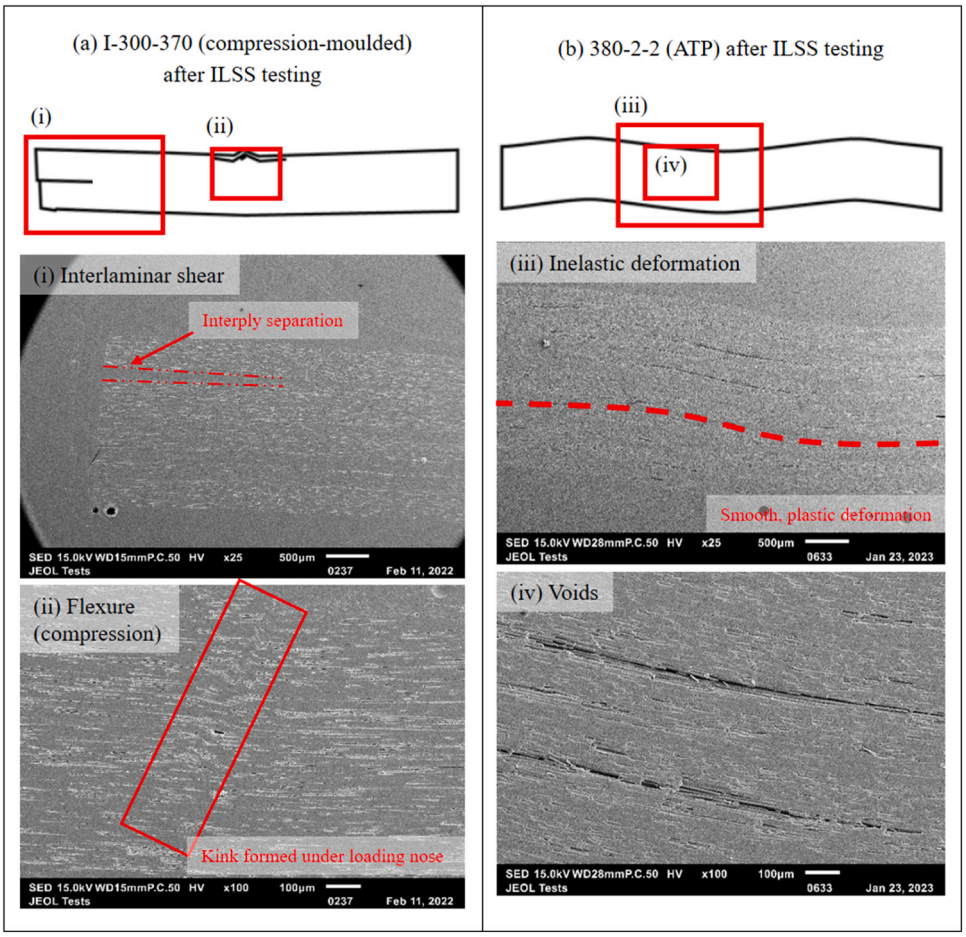

Fig. 14. Schematics and SEM images of cast ILSS specimens extracted from (a) I-300–370 (compression moulded) and (b) 380–2–2 (ATP) with sketches highlighting failure modes. Images are of the side of the specimens.

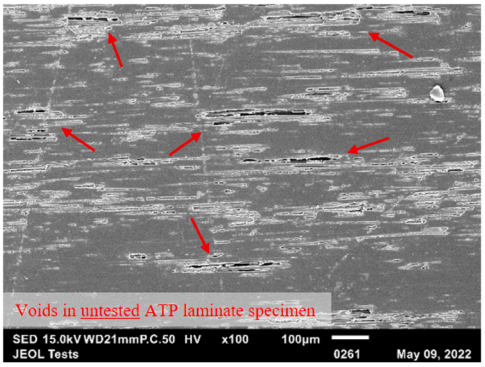

Fig. 15. SEM image of an untested ATP laminate sample showing intra-ply voids.

3.4. ATP manufacturing insights

As evidenced in Section 3, the ATP laminates studied displayed inferior performance when compared to the compression-moulded laminates in this work and other ATP-manufactured CF/PEEK laminates in literature, particularly in the case of flexural 0 ° testing. While PEEK has faster crystallisation kinetics than PEKK [3,15], which is generally beneficial for achieving higher crystallinities in ATP manufacturing, the results of the CF/PEKK laminates in this work show considerable scope for improvement. The underperformance is likely a consequence of suboptimal processing parameters, perhaps the most significant ones being the material temperature at nip and tool temperature (unheated). This was also apparent for CF/PEKK in Hoang et al.'s work [35] with an unheated tool, where with slightly higher nip temperatures (417–430 °C) than in the current study (370–390 °C), ILSS testing resulted in very similar values to the work presented in this article. Exposure to higher temperatures will lower polymer viscosity during tape placement, which could result in improved interply bonding and polymer chain reptation [44,45]. This was particularly evident in Stokes-Griffin et al.'s work on CF/PEEK [5], where nip temperatures significantly higher than melting temperature (400–600 °C, significantly higher than those used in this work) resulted in an ATP laminate performance comparable to autoclaved counterparts. It is worth noting, however, that PEEK is faster crystallising than PEKK, and therefore the fast cooling that the material undergoes in ATP manufacturing may be more adequate for PEEK than PEKK. Introducing a heated tool is likely to help with the material's exposure to higher temperatures, aiding with interply consolidation and crystallisation extent while working at lower nip temperatures. This was demonstrated in Esguerra-Arce et al.'s work [15], where using a heated tool at 200 °C reduced void content and improved the crystallinity of CF/PEKK. Saenz-Castillo et al.'s work on CF/PEEK [46] also observed similar results, where using similar nip temperatures to this study but with a heated tool at 200 °C resulted in an ILSS performance close to autoclaved samples.

Literature has highlighted, however, the problem of void rebound if the material is held at higher temperatures once roller pressure is removed (the re-emergence of pre-existing voids after these have been compressed during tape lay-down) [6,44,47]. This therefore poses conflicting mechanisms for PEKK, where high temperatures and slow

Table 6
ILSS results in this work and in literature.

Material	Autoclave	Laser ATP					
	ILSS (MPa)	Nip temp (°C)	Tool temperature (°C)	Tool material	Lay-down speed (m/min)	Roller pressure/load	ILSS (MPa)
IMS65/PEEK[12]	105	380	Unheated	Aluminium	3	2.5 bar	42.5
AS4D/PEKK[35]	~90	417	Unheated	Not specified	2.4	1000 N	~20
		430	Unheated	Not specified	2.4	1000 N	~20
		430	Unheated	Not specified	6	1000 N	~20
This work, AS7/PEKK	93–101 (compression moulding)	370	Unheated	Mild steel	4	2 bar	22.0
		380	Unheated	Mild steel	4	2 bar	24.4
		390	Unheated	Mild steel	4	2 bar	29.3
		380	Unheated	Mild steel	2	2 bar	27.0
		380	Unheated	Mild steel	4	4 bar	26.6

cooling are desirable for adequate crystallinity levels and interply chain reptation, but prolonged exposure to temperatures above T_g with no consolidation pressure may result in void rebound. Further to this, high lay-down speeds have been shown to not offer sufficient compaction time to achieve a good interply bond [47]. This requires an optimisation exercise of material temperature, tool temperature, lay-down speed and roller pressure, to establish optimal parameters regarding exposure to heat and compressive loads, and achieve acceptable levels of crystallinity, interply consolidation and void reduction for the composite material in question. These parameters will be highly dependent on the material type and its inherent crystallisation ability, average molecular weight and molecular weight distribution, and polydispersity index. Lamontia and Gruber [9] have suggested a modular lay-down head providing further heating, compaction and cooling steps, however these result in bulkier equipment pieces which may limit the equipment's ability to manufacture geometrically complex shapes, which is an attractive quality of ATP manufacturing.

4. Conclusions

In this work, CF/PEKK laminates were processed using different cycles under compression moulding (holding temperatures in the melt of 370 and 380 °C, followed by isothermal holds of 220, 260 and 300 °C or a cooling rate of 5 °C/min) and ATP (nip temperatures of 370, 380 and 390 °C, lay-down speeds of 2 and 4 m/min, and roller pressures of 2 and 4 bar). Their consolidation quality, crystallinity development in the matrix and flexural and interlaminar performance were evaluated. Overall, it was observed that compression-moulded laminates achieved a very good consolidation and all compression-moulded laminates performed similarly regardless of their processing history, with a marginally higher transverse flexural performance of the laminate manufactured at a higher holding temperature in the melt. The highest extent of crystallinity development was achieved across all the compression-moulded laminates. Differences were observed in their morphology as expected by general polymeric theory, where higher isothermal temperatures result in a lower nucleation density and therefore larger spherulitic entities. Chemical etching to expose these structures also highlighted the potential presence of a transcrystalline region at the fibre-matrix interface that the chemical etching attacked more aggressively.

Comparing the ATP laminates' performance with the compression-moulded laminates showed overall lower properties and quality. This is expected, due to the differences between the two processing techniques. The more rapid heating and cooling in the ATP manufacturing process resulted in poor consolidation quality, a higher void content, lower crystallinity and a significant reduction in mechanical performance. This is more prominent in slower crystallising PEKK than that in faster crystallising PEEK-based composites. In this study, increasing the nip temperature in ATP manufacturing had the most noticeable effect on mechanical performance, followed by a slower lay-down speed resulting in a lower void content and a marginal increase in both mechanical performance and crystallinity. However, these differences were not significant when compared to the performance of the compression-moulded laminates. Optimising the parameters of ATP manufacturing to better suit the PEKK matrix would likely improve all of the above properties. Specifically, the use of a higher temperature at nip and the use of a heated tool is likely to improve the consolidation quality and crystallinity of ATP laminates; and a higher roller pressure may contribute to void content reduction.

CRediT authorship contribution statement

Helena Pérez-Martín: Conceptualisation, Investigation, Formal analysis, Project administration, Writing – original draft. **Stefan Buchalik-Bopp:** Investigation, Resources, Writing – review & editing. **Barbara E. Guettler:** Supervision, Resources, Writing – review & editing. **Paul Mackenzie:** Supervision, Resources, Writing – review & editing. **Alex Baidak:** Supervision, Resources, Writing – review & editing. **Conchúr M. Ó Brádaigh:** Supervision, Resources, Writing – review & editing. **Dipa Ray:** Conceptualisation, Supervision, Resources, Project administration, Writing – review & editing.

Declaration of Competing Interest

The authors declare that they have no known competing financial interests or personal relationships that could have appeared to influence the work reported in this paper.

Data availability

Data will be made available on request.

Acknowledgements

The authors acknowledge the financial support received from the National Manufacturing Institute for Scotland (NMIS-IDP/009) and Hexcel Composites Limited. The authors would also like to thank Ms. Pia Eichert at the Leibniz-Institut für Verbundwerkstoffe GmbH for their support and thermal analysis facilities; as well as Mr. David Jones for their help in manufacturing the ATP laminate at the University of Limerick.

References

[1] T. Choupin, B. Fayolle, G. Régnier, C. Paris, J. Cinquin, B. Brulé, Isothermal crystallization kinetic modeling of poly(etherketoneketone) (PEKK) copolymer, Polymer 111 (2017) 73–82, https://doi.org/10.1016/j.polymer.2017.01.033.
[2] L. Quiroga Cortés, N. Caussé, E. Dantras, A. Lonjon, C. Lacabanne, Morphology and dynamical mechanical properties of poly ether ketone ketone (PEKK) with meta phenyl links, J. Appl. Polym. Sci. 133 (2016) 1–10, https://doi.org/10.1002/app.43396.
[3] H. Pérez-Martín, P. Mackenzie, A. Baidak, C.M. Ó Brádaigh, D. Ray, Crystallinity studies of PEKK and carbon fibre/PEKK composites: A review, Compos Part B Eng. 223 (2021), 109127, https://doi.org/10.1016/j.compositesb.2021.109127.

[4] S.Z.D. Cheng, R.M. Ho, B.S. Hsiao, K.H. Gardner, Polymorphism and crystal structure identification in poly(aryl ether ketone ketone)s, Macromolecules 197 (1996) 185–213, https://doi.org/10.1002/macp.1996.021970115.

[5] C.M. Stokes-Griffin, P. Compston, The effect of processing temperature and placement rate on the short beam strength of carbon fibre-PEEK manufactured using a laser tape placement process, Compos Part Appl. Sci. Manuf. 78 (2015) 274–283, https://doi.org/10.1016/j.compositesa.2015.08.008.

[6] A.J. Comer, D. Ray, W.O. Obande, D. Jones, J. Lyons, I. Rosca, et al., Mechanical characterisation of carbon fibre–PEEK manufactured by laser-assisted automated-tape-placement and autoclave, Compos Part Appl. Sci. Manuf. 69 (2015) 10–20, https://doi.org/10.1016/j.compositesa.2014.10.003.

[7] A. Beehag, L. Ye, Role of cooling pressure on interlaminar fracture properties of commingled CF/PEEK composites, Compos Part Appl. Sci. Manuf. 27 (1996) 175–182, https://doi.org/10.1016/1359-835X(95)00027-Y.

[8] J.P. Kilroy, C.M. Ó Brádaigh, C.O.A. Semprimoschnig, Mechanical and physical evaluation of a new carbon fibre/PEEK composite system for space applications, SAMPE J. (2008) 1–12.

[9] M. Lamontia, M. Gruber, Remaining developments required for commercializing in situ thermoplastic ATP, SAMPE Eur. Conf. (2007) 1–15.

[10] Z. Qureshi, T. Swait, R. Scaife, H.M. El-Dessouky, In situ consolidation of thermoplastic prepreg tape using automated tape placement technology: potential and possibilities, Compos Part B Eng. 66 (2014) 255–267, https://doi.org/10.1016/j.compositesb.2014.05.025.

[11] F. Shadmehri, S.V. Hoa, J. Fortin-Simpson, H. Ghayoor, Effect of in situ treatment on the quality of flat thermoplastic composite plates made by automated fiber placement (AFP, Adv. Manuf. Polym. Compos Sci. 4 (2018) 41–47, https://doi.org/10.1080/20550340.2018.1444535.

[12] A. Chanteli, A.K. Bandaru, D. Peeters, R.M. O'Higgins, P.M. Weaver, Influence of repass treatment on carbon fibre-reinforced PEEK composites manufactured using laser-assisted automatic tape placement, Compos Struct. 248 (2020), 112539, https://doi.org/10.1016/j.compstruct.2020.112539.

[13] J. Denault, M. Dumouchel, Consolidation Process of PEEK/Carbon Composite for Aerospace Applications, Adv. Perform. Mater. 5 (1998) 83–96, https://doi.org/10.1023/A:1008638105370.

[14] K. Kozaczuk, Automated fiber placement systems overview, Trans. Inst. Aviat. 245 (2016) 52–59, https://doi.org/10.5604/05096669.1226355.

[15] Esguerra-Arce I., Martín M.I., Pérez-Pastor A., García-Martínez V. Evolution of crystallinity with multiple lamination steps in high performance thermoplastic composites by in-situ consolidation process. Twenty-Second Int Conf Compos Mater, 2019.

[16] T. Choupin, B. Fayolle, G. Régnier, C. Paris, J. Cinquin, B. Brulé, A more reliable DSC-based methodology to study crystallization kinetics: Application to poly(ether ketone ketone) (PEKK) copolymers, Polymer 155 (2018) 109–115, https://doi.org/10.1016/j.polymer.2018.08.060.

[17] K.C.H. Gardner, B.S. Hsiao, R.R. Matheson, B.A. Wood, Structure, crystallization and morphology of poly (aryl ether ketone ketone, Polymer 33 (1992) 2483–2495, https://doi.org/10.1016/0032-3861(92)91128-O.

[18] R.M. Ho, S.Z.D. Cheng, B.S. Hsiao, K.H. Gardner, Crystal morphology and phase identifications in poly(aryl ether ketone)s and their copolymers. 1. Polymorphism in PEKK, Macromolecules 27 (1994) 2136–2140, https://doi.org/10.1021/ma00086a023.

[19] I.Y. Chang, B.S. Hsiao, Thermal properties of high performance thermoplastic composites based on poly(ether ketone ketone) (PEKK), 36th Int SAMPE Symp. (1991) 1587–1601.

[20] H. Pérez-Martín, P. Mackenzie, A. Baidak, C.M. Ó Brádaigh, D. Ray, Crystallisation behaviour and morphological studies of PEKK and carbon fibre/PEKK composites, Compos Part Appl. Sci. Manuf. 159 (2022), 106992, https://doi.org/10.1016/j.compositesa.2022.106992.

[21] L. Jin, J. Ball, T. Bremner, H.-J. Sue, Crystallization behavior and morphological characterization of poly(ether ether ketone, Polymer 55 (2014) 5255–5265, https://doi.org/10.1016/j.polymer.2014.08.045.

[22] D.C. Bassett, R.H. Olley, I.A.M. Al Raheil, On crystallization phenomena in PEEK, Polymer 29 (1988) 1745–1754, https://doi.org/10.1016/0032-3861(88)90386-2.

[23] E. Bessard, O. De Almeida, G. Bernhart, Unified isothermal and non-isothermal modelling of neat PEEK crystallization, J. Therm. Anal. Calor. 115 (2014) 1669–1678, https://doi.org/10.1007/s10973-013-3308-8.

[24] D.J. Blundell, B.N. Osborn, The morphology of poly(aryl-ether-ether-ketone, Polymer 24 (1983) 953–958, https://doi.org/10.1016/0032-3861(83)90144-1.

[25] M.P. Lattimer, J.K. Hobbs, M.J. Hill, P.J. Barham, On the origin of the multiple endotherms in PEEK, Polymer 33 (1992) 3971–3973, https://doi.org/10.1016/0032-3861(92)90391-9.

[26] Y. Lee, R.S. Porter, J.S. Lin, On the double-melting behavior of poly(ether ether ketone, Macromolecules 22 (1989) 1756–1760, https://doi.org/10.1021/ma00194a043.

[27] B.S. Hsiao, I.Y. Chang, B.B. Sauer, Isothermal crystallization kinetics of poly(ether ketone ketone) and its carbon-fibre-reinforced composites, Polymer 32 (1991) 2799–2805, https://doi.org/10.1016/0032-3861(91)90111-U.

[28] S. Tencé-Girault, J. Quibel, A. Cherri, S. Roland, B. Fayolle, S. Bizet, et al., Quantitative Structural Study of Cold-Crystallized PEKK, ACS Appl. Polym. Mater. 3 (2021) 1795–1808, https://doi.org/10.1021/acsapm.0c01380.

[29] B.S. Hsiao, K.H. Gardner, S.Z.D. Cheng, Crystallization of poly(aryl ether ketone ketone) copolymers containing terephthalate/isophthalate moieties, J. Polym. Sci. Part B Polym. Phys. 32 (1994) 2585–2594, https://doi.org/10.1002/polb.1994.090321604.

[30] J. Seo, X. Zhang, R.P. Schaake, A.M. Rhoades, R.H. Colby, Dual Nakamura model for primary and secondary crystallization applied to nonisothermal crystallization of poly(ether ether ketone, Polym. Eng. Sci. 61 (2021) 2416–2426, https://doi.org/10.1002/pen.25767.

[31] S.-L. Gao, J.-K. Kim, Cooling rate influences in carbon fibre/PEEK composites. Part I. Crystallinity and interface adhesion, Compos Part Appl. Sci. Manuf. 31 (2000) 517–530, https://doi.org/10.1016/S1359-835X(00)00009-9.

[32] S. Saiello, J. Kenny, L. Nicolais, Interface morphology of carbon fibre/PEEK composites, J. Mater. Sci. 25 (1990) 3493–3496, https://doi.org/10.1007/BF00575375.

[33] Weiss R. Influence of production parameters on the mechanical behaviour of CF/PEEK. Dev. Sci. Technol. Compos. Mater., Stuttgart: 1990, p. 1007–12.

[34] Y. Lee, R.S. Porter, Crystallization of poly(etheretherketone) (PEEK) in carbon fiber composites, Polym. Eng. Sci. 26 (1986) 633–639, https://doi.org/10.1002/pen.760260909.

[35] V.-T. Hoang, B.-S. Kwon, J.-W. Sung, H.-S. Choe, S.-W. Oh, S.-M. Lee, et al., Postprocessing method-induced mechanical properties of carbon fiber-reinforced thermoplastic composites, J. Thermoplast. Compos Mater. 36 (2023) 432–447, https://doi.org/10.1177/0892705720945376.

[36] D.J. Blundell, R.A. Crick, B. Fife, J. Peacock, A. Keller, A. Waddon, Spherulitic morphology of the matrix of thermoplastic PEEK/carbon fibre aromatic polymer composites, J. Mater. Sci. 24 (1989) 2057–2064, https://doi.org/10.1007/BF02385421.

[37] M.A. Lamontia, M.B. Gruber, A. Systems, S. Drive, J. Tierney, J.W. Gillespie, Modeling the Accudyne Thermoplastic In Situ ATP Process, Proc. SAMPE Conf. (2009) 8.

[38] Schledjewski R., Miaris A. Thermoplastic tape placement by means of diode laser heating. vol. 54, 2009.

[39] Chen J., Yousefpour A., Hojjati M., Cai X., Hoa S. Automated fiber placement of thermoplastic composites—lessons learned, 2013.

[40] R.M. Ho, S.Z.D. Cheng, B.S. Hsiao, K.H. Gardner, Crystal morphology and phase identifications in poly(aryl ether ketone)s and their copolymers. 3. Polymorphism in a polymer containing alternated terephthalic acid and isophthalic acid isomers, Macromolecules 28 (1995) 1938–1945, https://doi.org/10.1021/ma00110a030.

[41] X. Tardif, B. Pignon, N. Boyard, J.W.P. Schmelzer, V. Sobotka, D. Delaunay, et al., Experimental study of crystallization of PolyEtherEtherKetone (PEEK) over a large temperature range using a nano-calorimeter, Polym. Test. 36 (2014) 10–19, https://doi.org/10.1016/j.polymertesting.2014.03.013.

[42] S. Risteska, A.T. Petkoska, S. Samak, M. Drienovsky, Annealing Effects on the Crystallinity of Carbon Fiber-Reinforced Polyetheretherketone and Polyohenylene Laminate Composites Manufactured by Laser Automatic Tape Placement, Mater. Sci. 26 (2020) 308–316, https://doi.org/10.5755/j01.ms.26.3.21489.

[43] A. Beehag, L. Ye, Influence of cooling rate on interlaminar fracture properties of unidirectional commingled CF/PEEK composites, Appl. Compos Mater. 2 (1995) 135–151, https://doi.org/10.1007/BF00567748.

[44] Gruber M.B., Lockwood I.Z., Dolan T.L., Funck S.B., Tierney J.J., Simacek P., et al. Thermoplastic in situ placement requires better impregnated tapes and tows. Int SAMPE Tech Conf, 2012.

[45] A. Deignan, W.F. Stanley, M. McCarthy, Insights into wide variations in carbon fibre/polyetheretherketone rheology data under automated tape placement processing conditions, J. Compos Mater. 52 (2018) 2213–2228, https://doi.org/10.1177/0021998317740733.

[46] D. Saenz-Castillo, M.I. Martín, S. Calvo, F. Rodríguez-Lence, A. Güemes, Effect of processing parameters and void content on mechanical properties and NDI of thermoplastic composites, Compos Part Appl. Sci. Manuf. (2019), https://doi.org/10.1016/j.compositesa.2019.03.035.

[47] G. Clancy, D. Peeters, V. Oliveri, D. Jones, R.M. O'Higgins, P.M. Weaver, A study of the influence of processing parameters on steering of carbon fibre/PEEK tapes using laser-assisted tape placement, Compos Part B Eng. 163 (2019) 243–251, https://doi.org/10.1016/j.compositesb.2018.11.033.